Acta Crystallographica Section B
Structural Science
ISSN 0108-7681

Ternary fluorides BaMF$_4$ (M = Zn, Mg and Mn) at low temperatures

Jose Maria Posse,* Andrzej Grzechnik and Karen Friese

Departamento Física Materia Condensada, Universidad del País Vasco, Apdo 644, 48080 Bilbao, Spain

Correspondence e-mail: josemaria@wm.lc.ehu.es

Received 29 May 2009
Accepted 10 July 2009

Ternary fluorides BaMF$_4$ (M = Zn, Mg, Mn) have been studied in the temperature range from 300 to 10 K using synchrotron and laboratory powder and single-crystal diffraction. The first two compounds are stable down to 10 K, while the third one undergoes a phase transition to an incommensurately modulated structure at approximately 250 K. The modulated phase is stable down to 10 K. The magnetic anomalies at 45 and 27 K observed previously in BaMnF$_4$ are exclusively reflected in the behavior of the γ component of the **q** vector, which assumes an irrational value of approximately 0.395 Å^{-1} at the temperature corresponding to the onset of the magnetic ordering and then stays constant down to 10 K. Mn—Mn distances do not indicate any structural response to the magnetic ordering. The formation of the modulated phase can be explained on the basis of simple geometrical criteria. The incorporation of the large Mn cation in the octahedral sheets implies an increase of the cavity in which the Ba ion is incorporated. This leads to the formation of the modulated structure to adapt the coordination sphere around Ba in such a way that the bond-valence sums can be kept close to the ideal value of two. With further lowering of the temperature, the charge balance around the Ba ion requires an increasingly anharmonic character of the modulation function of Ba, until finally at 10 K a crenel-like shape is assumed for the modulation of this atom.

1. Introduction

Ternary fluorides with the general formula BaMF$_4$ (M = Mn, Zn, Mg, Fe, Ni, Cu or Co) crystallize in the space group $Cmc2_1$ (Z = 4; Keve *et al.*, 1969; von Schnering & Bleckmann, 1968; Sciau *et al.*, 1988; Lapasset *et al.*, 1996; Gingl, 1997; Gredin *et al.*, 1996; Welsch *et al.*, 1999). The M ions are surrounded by six F atoms forming corner-sharing octahedral layers perpendicular to [010] (Fig. 1). Between these layers the Ba ions, which are coordinated by nine F atoms, are allocated. In general, the unit-cell volumes of the BaMF$_4$ compounds depend on the ionic radius of the M^{2+} cation (Fig. 2). In the compounds BaBeF$_4$ (Werner & Kubel, 2005) and BaPdF$_4$ (Müller & Hoppe, 1972), the ionic radius of the M cations is either too small or too large to be octahedrally coordinated and the coordination around the M cation changes to tetrahedral or square planar.

All the BaMF$_4$ compounds are piezoelectric at ambient conditions. Owing to their higher transparency when compared with oxides, these fluorides can be used as optical materials (Villora *et al.*, 2007; Zeng *et al.*, 2007; Kannan *et al.*, 2008). The extrapolated transition temperatures to a hypothetic paraelectric phase were estimated to lie above the melting points (Didomenico *et al.*, 1969). Some of the BaMF$_4$

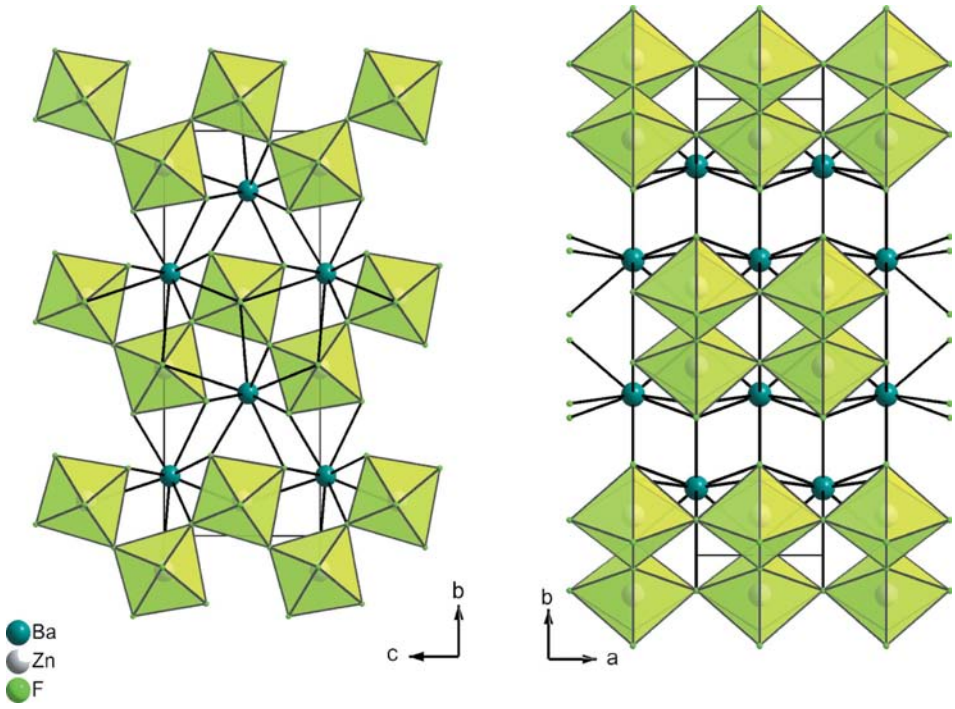

Figure 1
Crystal structure of $BaZnF_4$ at room temperature. Octahedra around the Zn atoms are drawn.

compounds (M = Mn, Fe, Co or Ni) exhibit multiferroic behaviour (Ederer & Spaldin, 2006).

Temperature-dependent Raman experiments performed on $BaZnF_4$ by Bordallo *et al.* (1994) showed anomalies which were interpreted as being due to the existence of bi-dimensional disorder perpendicular to the octahedral layers. These observations motivated X-ray diffraction measurements as a function of temperature focused on the study of diffuse scattering (Almairac *et al.*, 1995), which was attributed to the arrangement of octahedra in bi-dimensional clusters. In later inelastic neutron scattering experiments by Almairac *et al.* (1997), an unexplained shift of the minimum of the phonon branch at the point R was observed. It was concluded that the $BaMF_4$ compounds are structurally unstable at low temperatures. Until now, this instability has only been confirmed for $BaMnF_4$, which transforms to an incommensurately modulated phase at temperatures below 250 K described by Sciau *et al.* (1988), Scott (1979), Hidaka *et al.* (2001) and Yoshimura & Hidaka (2005).

Below T_N = 27 K, $BaMnF_4$ shows antiferromagnetic ordering of the Mn^{2+} spins. According to earlier investigations (Holmes *et al.*, 1969; Samara & Scott, 1977; Tsuboi & Kleemann, 1983; Schaefer *et al.*, 1983) the spins are slightly canted from the b axis and weak ferromagnetism occurs below T_N. The ferromagnetism is related to the linear or quadratic magnetoelectric effect induced by the correlations between the magnetic and electric properties. Between 27 and 45 K an intermediate magnetic phase is observed characterized by preponderant in-plane spin ordering along the b axis.

However, a more recent result (Yoshimura *et al.*, 2006) suggests that the spins are uniaxially aligned parallel to the b axis and no weak ferromagnetic component is apparent below 27 K. In addition, the intermediate magnetic phase, characterized by plane-like magnetic diffuse scattering, is interpreted as showing one-dimensional antiferromagnetic spin order of Mn^{2+} (Yoshimura *et al.*, 2006).

The dilution of the paramagnetic Mn^{2+} with diamagnetic Zn^{2+} in the solid solution $BaMn_{1-x}Zn_xF_4$ leads to a suppression of the antiferromagnetic ordering (Veira *et al.*, 2008). Furthermore, the temperature of the structural phase transition to the incommensurate phase also decreases, an effect which can be attributed to the smaller size of the Zn^{2+} cation when compared with Mn^{2+}. Eventually, at x = 0.75 the incommensurate phase is suppressed.

We are generally interested in the pressure–temperature stability of ferroic fluoride compounds. Here our aim is to further investigate the possibility of structural instabilities in $BaMgF_4$, $BaZnF_4$ and $BaMnF_4$ using thermal analysis and X-ray diffraction at low temperatures. We are especially interested in the structure of the incommensurate phase of $BaMnF_4$ at temperatures below 100 K and in the response of the structure to the onset of magnetic ordering.

For the future we plan comparable studies on the pressure-dependent behaviour of $BaMF_4$ compounds.

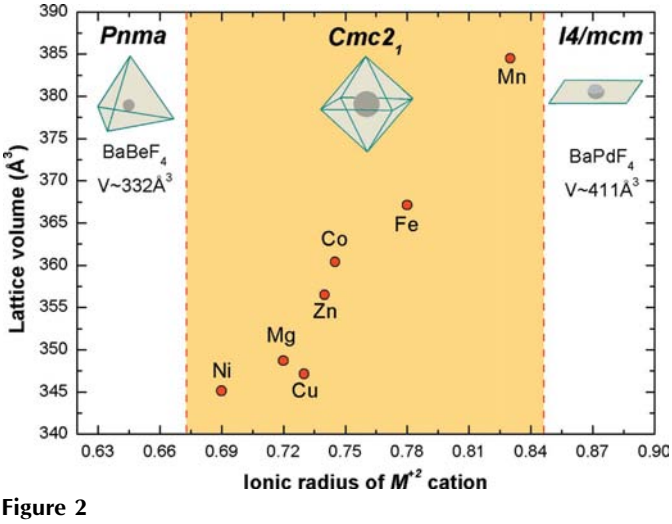

Figure 2
Unit-cell volumes as a function of the ionic radius of the M cation in the $BaMF_4$ compounds.

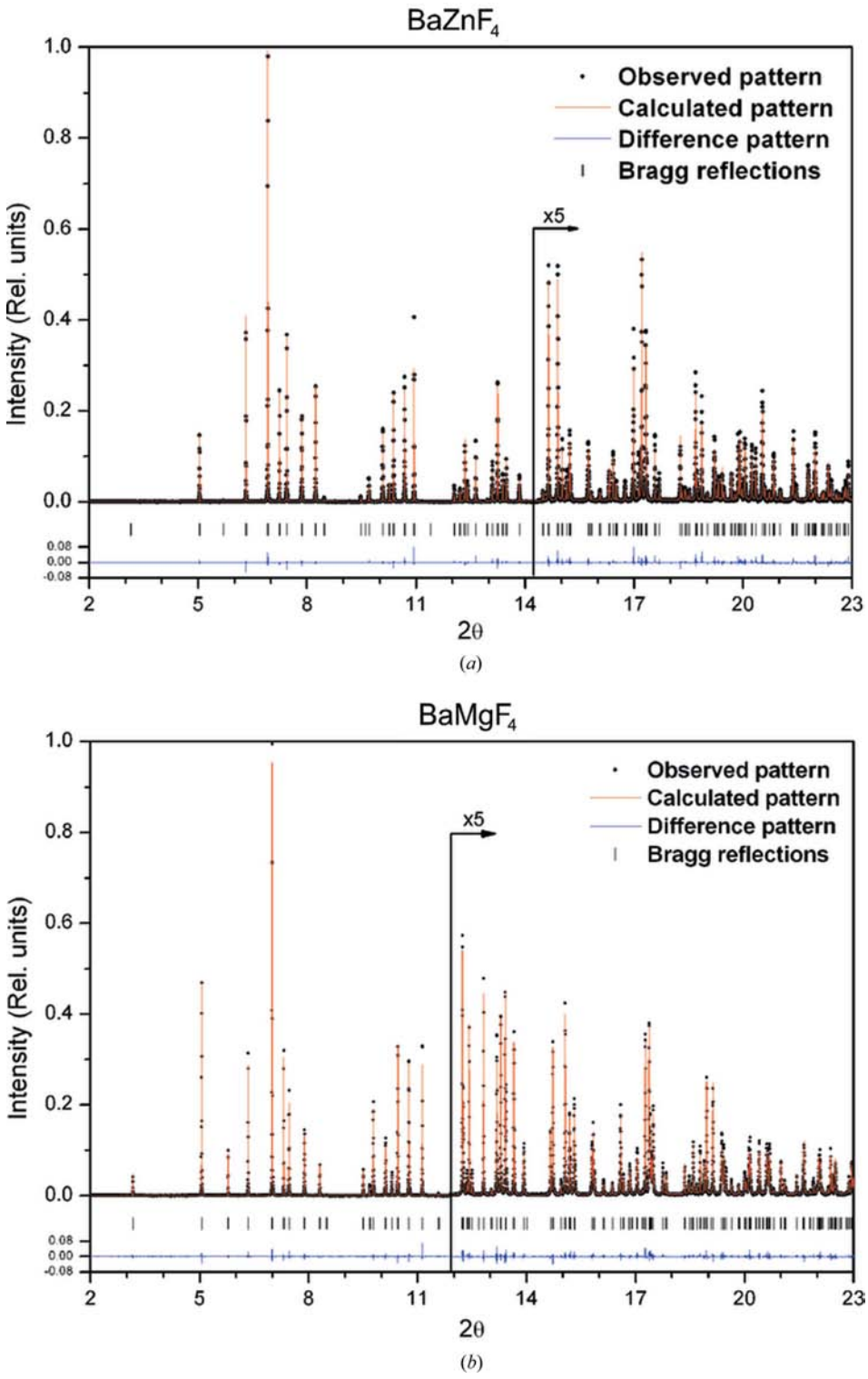

Figure 3
Observed, calculated and difference powder X-ray patterns of $BaZnF_4$ and $BaMgF_4$ at 10 K.

2. Experimental methods

Large single crystals ($> 0.5\ cm^3$) of $BaMgF_4$, $BaZnF_4$ and $BaMnF_4$ were grown with the Czochralski method. Small fragments of each crystal were ground for thermal analysis and powder X-ray diffraction experiments.

Differential scanning calorimetry was carried out using the systems Pyris 1 and 7 (Perkin–Elmer) in the temperature range 100–300 K.

Powder X-ray diffraction data ($\lambda = 0.3995$ Å) were collected using 0.9 mm capillaries down to 10 K (a liquid-helium cryostat Janis) on the beamline ID31 at the European Synchrotron Radiation Facility (Grenoble).

Single-crystal X-ray diffraction measurements were carried out using different diffractometers and cryostats:

(i) Stoe IPDS-II (Mo $K\alpha$; N_2 cryostat: 100–295 K) – $BaMgF_4$;

(ii) Stoe IPDS-II ($\lambda = 0.75$ Å), SCD beamline, Institute for Synchrotron Radiation, ANKA Karlsruhe; N_2 cryostat: 100–295 K – $BaZnF_4$ and $BaMnF_4$;

(iii) Oxford Diffraction Xcalibur-2 (Mo $K\alpha$; Helijet: 10–50 K) – $BaZnF_4$ and $BaMnF_4$.

Structural refinements of the powder and single-crystal X-ray diffraction data were performed using the program *JANA*2006 (Petříček *et al.*, 2006).

3. Experimental results and structure refinements

3.1. $BaMgF_4$ and $BaZnF_4$

The data obtained by the differential scanning calorimetry technique on $BaZnF_4$ and $BaMgF_4$ in the range 100–300 K are smooth curves of heat flux *versus* temperature without any anomalies. The smooth curves indicate there is not any first-order phase transitions in these two materials.

All powder diagrams of both compounds measured as a function of temperature were refined with the Rietveld method in the space group $Cmc2_1$, which accounts for all the observed reflections. We did not detect any diffraction features that would suggest temperature-induced phase transitions between 10 and 290 K. The fully refined patterns collected at 10 K are shown in Fig. 3. Experimental details are given in Table 1; normalized lattice parameters as a

Table 1
Experimental details for Rietveld refinements of $BaMgF_4$, $BaZnF_4$ and $BaMnF_4$.

For all structures: $Z = 4$. Experiments were carried out at 10 K with synchrotron radiation, $\lambda = 0.3995$ Å. Refinement was with 0 restraints.

Compound	$BaMgF_4$	$BaZnF_4$	$BaMnF_4$
Crystal data			
M_r	237.6	278.7	268.3
Crystal system, (super)space group	Orthorhombic, $Cmc2_1$	Orthorhombic, $Cmc2_1$	Monoclinic, $X2_1(\frac{1}{2}\,\frac{1}{2}\,\gamma)$
a, b, c (Å)	4.11899 (1), 14.46260 (6), 5.81151 (3)	4.19057 (2), 14.51281 (6), 5.83568 (3)	4.19843 (1), 15.05570 (6), 6.00030 (3)
γ (°)	90	90	90.0849 (2)
q vector	–	–	$[\frac{1}{2}, \frac{1}{2}, 0.39462\ (4)]$
V (Å^3)	346.199 (3)	354.908 (3)	379.281 (4)
μ (mm^{-1})	2.483	3.734	2.825
Specimen shape, size (mm)	Cylinder, 0.7	Cylinder, 0.7	Cylinder, 0.7
Data collection			
Data collection method	ID31, ESRF, Grenoble	ID31, ESRF, Grenoble	ID31, ESRF, Grenoble
Specimen mounting	Quartz capillary	Quartz capillary	Quartz capillary
Data-collection mode	Transmission	Transmission	Transmission
Scan method	Continuous	Continuous	Continuous
2θ values (°)	$2\theta_{min} = 2.00$, $2\theta_{max} = 23.00$, $2\theta_{step} = 0.002$	$2\theta_{min} = 2.00$, $2\theta_{max} = 23.00$, $2\theta_{step} = 0.002$	$2\theta_{min} = 2.00$, $2\theta_{max} = 23.00$, $2\theta_{step} = 0.002$
No. of observed reflections	205	210	1078
$\sin\theta/\lambda$	0.4990	0.4990	0.4990
Refinement			
R_P	0.1154	0.1288	0.1116
wR_P	0.1776	0.2012	0.1693
R_{obs}	0.0249	0.0390	0.0501
wR_{obs}	0.0227	0.0329	0.3802
R_{all}	0.0265	0.0396	0.0577
wR_{all}	0.0228	0.0330	0.3802
No. of data points	14 983	14 983	14 984
No. of parameters	24	24	51

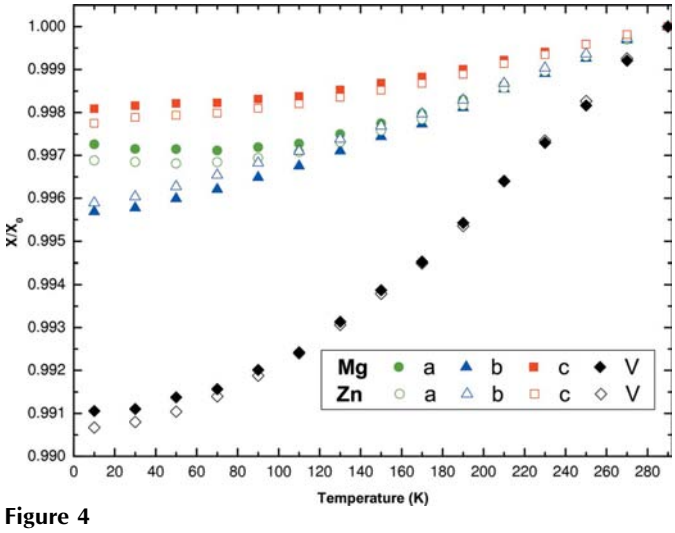

Figure 4
Temperature dependence of normalized lattice parameters and unit-cell volumes of $BaMgF_4$ and $BaZnF_4$.

function of temperature are portrayed in Fig. 4. Atomic coordinates and isotropic displacement parameters are accessible through the supplementary material.[1] The refined structural parameters were the atomic positions and isotropic displacement parameters. The pseudo-Voigt profile function (parameters GW and LY) was used during the refinements at all temperatures. We also refined anisotropic strain broadening parameters (St022 and St004; Stephens, 1999), a March–Dollase preferred orientation parameter in the direction [010], and a θ-zero offset.

The reciprocal space reconstruction based on the single-crystal data at all temperatures confirm the orthorhombic space group $Cmc2_1$ for both materials, without any violation of the corresponding extinction rules. In the reconstructions of reciprocal space we could not detect any diffuse scattering. Details of the single-crystal refinements are given in Table 2. Atomic coordinates and displacement parameters as a function of temperature have been deposited.

3.2. $BaMnF_4$

The powder diffraction diagrams of $BaMnF_4$ in the normal phase were refined with the Rietveld method in space group $Cmc2_1$ (Fig. 5). For the description of the modulated phase we used the space group $X2_1(\frac{11}{22}\gamma)$ with a non-conventional superspace centering $X = C' = (\frac{11}{22}0\frac{1}{2})$. This choice is based on two arguments: the X-centering leads to a monoclinic angle greater than 90° and the maintenance of the rational components of the **q** vector allows us to directly compare the structure of $BaMnF_4$ to those of the other two compounds of this study (Table 1).[2] The refined structural parameters taken into

[1] Supplementary data for this paper are available from the IUCr electronic archives (Reference: SN5085). Services for accessing these data are described at the back of the journal.

[2] This setting can be transformed to the superspace group $U{:}A2_111{:}111$ chosen by Sciau *et al.* (1988) by applying the transformations $a' = c$; $b' = 2b$; $c' = -2a$ and a subsequent change in the **q** vector according to $q' = (0, 1, -1) + q$.

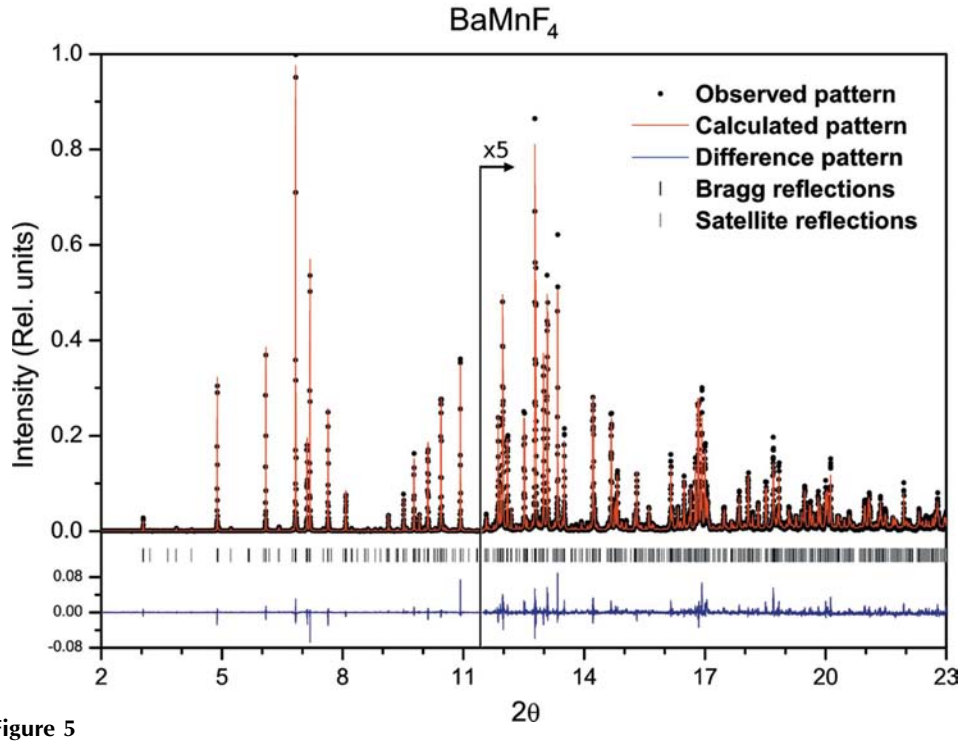

Figure 5
Observed, calculated and difference powder X-ray pattern of $BaMnF_4$ at 10 K.

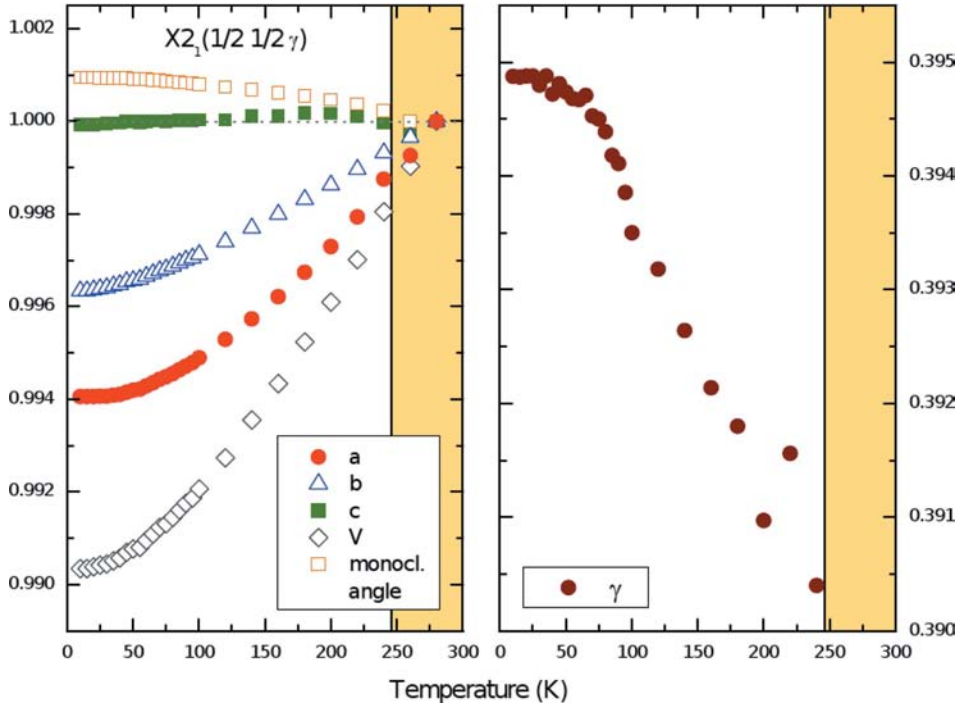

Figure 6
Temperature dependence of the lattice parameters (left) and the irrational component γ of the modulation vector (right) of $BaMnF_4$. The shaded regions indicate the stability region of the normal phase (space group $Cmc2_1$).

account in the Rietveld refinements were the atomic positions, isotropic displacement parameters and the first harmonics of the modulation amplitudes. The profile function was purely Lorentzian (parameter LY). As in the other two compounds we also refined anisotropic strain-broadening parameters (St0202 and St0040; Stephens, 1999), a March–Dollase preferred orientation parameter in the [010] direction, and a θ-zero offset.

We extracted the temperature-dependent behavior of the lattice parameter and the irrational component of the **q** vector (Fig. 6).

In addition, we refined the structure at 255, 245, 175, 100, 35 and 10 K from single-crystal data. The refinement at 255 K corresponds to the normal phase. At 245 K, below the phase transition to the incommensurate phase, the number of observed satellite reflections with $I>3\sigma$ was very small and we therefore limited the refinement to the parameters of the average structure. At lower temperatures we performed full refinements of the modulated structure using the superspace group described above.

An inspection of reciprocal space reconstructed on the basis of the measured frames showed that the crystal structure in the modulated phase was affected by twinning. The twin law is a mirror plane perpendicular to the crystallographic *b* axis, which has already been described for this compound in the literature (Sciau *et al.*, 1988; Ryan, 1986) and was taken into account in our refinement.[3] In our reconstructions of reciprocal space we observed no diffuse scattering. Details of the single-crystal measurements and refinements at the different temperatures are given in Table 3.

The refinement strategy can be summarized as follows: after anisotropic refinement of the average structure, we refined

[3] The introduction of additional inversion twinning always led to zero values for the individuals related *via* matrices with determinant −1.

Table 2
Experimental details for single-crystal refinements of $BaMgF_4$ and $BaZnF_4$.

$BaMgF_4$, space group $Cmc2_1$, $Z = 4$, $\lambda = 0.71073$ Å, refinement with 0 restraints				
Temperature (K)	250	200	150	100
Crystal data				
M_r	237.6	237.6	237.6	237.6
Crystal system	Orthorhombic	Orthorhombic	Orthorhombic	Orthorhombic
a, b, c (Å)	4.12743 (1), 14.51455 (6), 5.82028 (3)	4.12398 (2), 14.50096 (6), 5.81748 (3)	4.12099 (1), 14.48798 (6), 5.81496 (3)	4.11886 (2), 14.47610 (7), 5.81296 (4)
V (Å^3)	348.680 (2)	347.899 (2)	347.185 (2)	346.604 (2)
Radiation type	Mo $K\alpha$	Mo $K\alpha$	Mo $K\alpha$	Mo $K\alpha$
μ (mm^{-1})	11.50	11.46	11.48	11.56
ρ (g cm^{-3})	4.5254	4.5355	4.5449	4.5524
Crystal size	0.14 × 0.07 × 0.03	0.14 × 0.07 × 0.01	0.14 × 0.07 × 0.01	0.14 × 0.07 × 0.01
$hkl_{min} - hkl_{max}$	$\bar{6}\,\bar{2}\,\bar{1}\,\bar{8}$ – 6 2 1 8	$\bar{6}\,\bar{2}\,\bar{1}\,\bar{7}$ – 5 2 1 6	$\bar{6}\,\bar{2}\,\bar{1}\,\bar{7}$ – 5 2 1 8	$\bar{6}\,\bar{2}\,\bar{1}\,\bar{8}$ – 6 2 1 8
Data collection				
Data collection method	ω scans	ω scans	ω scans	ω scans
Absorption correction	Numerical	Numerical	Numerical	Numerical
T_{min}, T_{max}	0.367, 0.533	0.401, 0.534	0.316, 0.532	0.278, 0.531
No. of measured, independent and observed [$I > 3\sigma(I)$] reflections	2375, 617, 613	1609, 556, 554	1738, 625, 620	2112, 653, 647
Extinction coefficient	0.07 (1)	0.05 (1)	0.032 (4)	0.044 (4)
$R_{int}>3\sigma$	0.031	0.024	0.018	0.018
R_{int}(all)	0.031	0.024	0.018	0.018
Refinement				
R(obs), wR(obs)	0.0196, 0.0263	0.0171, 0.0270	0.0108, 0.0168	0.0118, 0.0168
R(all), wR(all)	0.0197, 0.0263	0.0172, 0.0270	0.0110, 0.0169	0.0120, 0.0169
g.o.f(all)	2.52	2.57	1.58	1.60
g.o.f(obs)	2.51	2.56	1.58	1.60
No. of reflections	617	556	625	653
No. of parameters	37	37	37	37
$\Delta\rho_{max}$, $\Delta\rho_{min}$ (e Å^{-3})	0.65, −0.71	0.61, −0.61	0.46, −0.44	0.49, −0.50
Absolute structure	Inversion	Inversion	Inversion	Inversion
Flack parameter	0.00 (5)	0.00 (5)	0.00 (5)	0.00 (5)

$BaZnF_4$, space group $Cmc2_1$, $Z = 4$, refinement with 0 restraints						
	$\lambda = 0.75$ Å				$\lambda = 0.71073$ Å	
Temperature (K)	290	200	150	100	50	10
Crystal data						
M_r	278.7	278.7	278.7	278.7	278.7	278.7
Crystal system	Orthorhombic	Orthorhombic	Orthorhombic	Orthorhombic	Orthorhombic	Orthorhombic
a, b, c (Å)	4.20369 (2), 14.57275 (7), 5.84817 (3)	4.19684 (3), 14.55067 (11), 5.84241 (4)	4.19350 (2), 14.53894 (7), 5.83952 (3)	4.19110 (2), 14.52846 (8), 5.83737 (3)	4.19029 (2), 14.51842 (7), 5.83613 (3)	4.19057 (2), 14.51281 (6), 5.83568 (3)
V (Å^3)	358.259 (2)	356.774 (2)	356.028 (2)	355.442 (2)	355.048 (2)	354.912
Radiation type	Synchrotron	Synchrotron	Synchrotron	Synchrotron	Mo $K\alpha$	Mo $K\alpha$
μ (mm^{-1})	20.54	20.63	20.67	20.71	17.71	17.71
ρ (g cm^{-3})	5.1657	5.1872	5.198	5.2066	5.2124	5.2144
Crystal size	0.02 × 0.02 × 0.01	0.02 × 0.02 × 0.01	0.02 × 0.02 × 0.01	0.02 × 0.02 × 0.01	0.16 × 0.10 × 0.05	0.16 × 0.10 × 0.05
$hkl_{min} - hkl_{max}$	$\bar{5}\,\bar{2}\,\bar{3}\,\bar{9}$ – 6 2 3 9	$\bar{5}\,\bar{2}\,0\,\bar{8}$ – 5 2 0 6	$\bar{4}\,\bar{2}\,0\,\bar{7}$ – 5 2 0 8	$\bar{5}\,\bar{2}\,0\,\bar{8}$ – 5 2 0 7	$\bar{5}\,\bar{2}\,0\,\bar{4}$ – 4 2 4 9	$\bar{5}\,\bar{2}\,0\,\bar{4}$ – 4 2 4 9
Data collection						
Data-collection method	Rotation method	Rotation method	Rotation method	Rotation method	ω and φ scans	ω and φ scans
Absorption correction	Numerical	Numerical	Numerical	Numerical	Gaussian	Gaussian
T_{min}, T_{max}	0.480, 0.674	0.476, 0.623	0.539, 0.646	0.549, 0.709	0.181, 0.440	0.182, 0.440
No. of measured, independent and observed [$I > 3\sigma(I)$] reflections	3748, 901, 827	1111, 484, 458	954, 537, 502	1944, 541, 522	2881, 538, 521	2878, 538, 524
Extinction coefficient	0.049 (5)	0.015 (7)	0.040 (7)	0.012 (4)	0.017 (2)	0.019 (2)
$R_{int}>3\sigma$	0.0944	0.1286	0.0888	0.0879	0.0469	0.0489
R_{int}(all)	0.0964	0.1289	0.1106	0.0891	0.0882	0.0469
Refinement						
R(obs), wR(obs)	0.0621, 0.0581	0.0612, 0.0688	0.0593, 0.0661	0.0366, 0.0404	0.0194, 0.0267	0.0219, 0.0284

Table 2 (continued)

$BaZnF_4$, space group $Cmc2_1$, $Z = 4$, refinement with 0 restraints						
	$\lambda = 0.75$ Å				$\lambda = 0.71073$ Å	
Temperature (K)	290	200	150	100	50	10
R(all), wR(all)	0.0710, 0.0590	0.0648, 0.0689	0.0628, 0.0663	0.0383, 0.0405	0.0203, 0.0268	0.0224, 0.0285
g.o.f(all)	3.65	5.13	4.32	3.10	1.94	1.89
g.o.f(obs)	3.54	4.99	4.18	3.06	1.96	1.87
No. of reflections	901	484	537	541	538	538
No. of parameters	37	37	37	37	37	37
$\Delta\rho_{max}$, $\Delta\rho_{min}$ (e Å^{-3})	3.17, −5.48; 0.012	3.33, −2.89	2.82, −3.57	2.16, −1.41	1.42, −0.99	1.94, −1.52
Absolute structure	Inversion twin	Inversion twin	Inversion twin	Inversion twin	Inversion twin	Inversion twin
Flack parameter	0.00 (5)	0.00 (5)	0.00 (5)	0.00 (5)	0.00 (5)	0.00 (5)

the amplitudes of the modulation functions up to the second and, at lower temperatures, up to the third harmonic. Modulation amplitudes which were smaller than three times the corresponding standard deviation were set to zero. An inspection of the Fourier maps around the Ba ions at a temperature of 10 K showed a strong anharmonic character of the modulation function, suggesting the use of a crenel function for this atom. Indeed, the introduction of the corresponding crenel function led to a significant improvement of the overall agreement factor of approximately 1%, while the number of parameters was not substantially increased. In particular, the wR(all) agreement factor for the second-order satellites dropped by nearly 4%, when the crenel function was introduced. At higher temperatures we did not observe a similar effect [the improvement of wR(all) for $m = 2$ reflections at 35 K is less than 0.2%] and therefore discarded the use of a crenel function.

At 35 and 10 K the anisotropic displacement parameters for Mn showed a tendency to turn negative (although within their standard deviation they remained positive) and we therefore decided to keep this atom isotropic. For reasons of consistency we also kept the F atoms at these temperatures isotropic. Trial refinements showed that the anisotropic treatment of these atoms does not improve the fit significantly at these low temperatures. Atomic coordinates, isotropic displacement parameters and amplitudes of the modulation functions are accessible through the supplementary material.

4. Discussion

The lattice parameters and unit-cell volume at 290 K for $BaMgF_4$ and $BaZnF_4$ are $a = 4.13031$ (2), $b = 14.52527$ (1), $c = 5.82267$ (5) Å, $V = 349.325$ (6) Å^3, and $a = 4.20358$ (2), $b = 14.57271$ (1), $c = 5.84819$ (5) Å, $V = 358.254$ (6) Å^3. Their temperature dependencies between 10 and 290 K extracted from the powder X-ray diffraction data are very similar, as seen in Figs. 4. (A table of the lattice parameters is provided in the supplementary material.) The relative thermal expansion is the largest along the b direction, but it never exceeds 0.5%. The a-lattice parameters exhibit a slight negative thermal expansion below approximately 50 K, while the temperature dependencies of the c-lattice parameters have sigmoidal-like shapes.

Neither our powder nor our single-crystal data provide a definite answer to the nature of the anomalous thermal behavior of the lattice parameters, as the standard deviation of bond distances and bond angles extracted from the structure refinements are too large to identify any significant trends as a function of temperature. Nevertheless, the analysis of the temperature dependence of the structures of $BaMgF_4$ and $BaZnF_4$ shows that in $BaMgF_4$ the octahedra get more regular when the temperature is decreased while in $BaZnF_4$ the changes in the octahedra with temperature are not significant. The negative thermal expansion observed in $BaZnF_4$ below 80 K (Fig. 4) might be related to the anomalies in the corresponding Raman spectra (Bordallo *et al.*, 1994), which are observed at similar temperatures. We do not observe the diffuse scattering which has previously been reported for $BaZnF_4$ by Almairac *et al.* (1995). However, one has to bear in mind that according to these authors the intensity of the diffuse scattering decreases as the temperature is lowered.

Our structural data on $BaMnF_4$ [lattice parameters at 280 K: $a = 4.223457$ (11), $b = 15.11086$ (5), $c = 6.00069$ (2) Å, and $V = 382.965$ (3) Å^3] confirm a structural phase transition to an incommensurate phase at 250 K. The transition is accompanied by a reduction of the symmetry from orthorhombic to monoclinic and involves the formation of a pseudomerohedral twin related to this loss of symmetry.

A comparison of the evolution of lattice parameter of $BaZnF_4$ and $BaMgF_4$ with $BaMnF_4$ shows striking differences (see also tables in the supplementary material). In the first two compounds the b axis, *i.e.* the direction perpendicular to the layers, is the one that contracts the most (Fig. 4) and thus the distance between adjacent octahedral layers is decreased. The a and c directions defining the octahedral layers decrease less. In contrast, in $BaMnF_4$ the lattice parameter that shrinks the most is the a-lattice parameter, *i.e.* one of the layer directions; at the same time the c-lattice parameter stays basically constant over the whole temperature range from 300 to 10 K (Fig. 6). On the other hand, the b-lattice parameter perpendicular to the layers shrinks to a degree comparable to that observed in $BaZnF_4$ and $BaMgF_4$. $BaMnF_4$ is the only one of the three compounds that shows a monoclinic distortion of the lattice, although the deviation from 90° is minimal and does not exceed 90.09° in the temperature range measured.

Within the stability region of the modulated phase of $BaMnF_4$ the γ value continuously increases with decreasing

Table 3
Experimental details of the single-crystal diffraction experiments on $BaMnF_4$ at different temperatures performed at the beamline SCD at ANKA, Karlsruhe (λ = 0.75 Å), and using an Oxford Xcalibur diffractometer with a laboratory source (λ = Mo $K\alpha$).

Lattice parameters and the γ component of the **q** vector are obtained from a LeBail fit of synchrotron powder data.

	ANKA SCD λ = 0.75 Å				Excalibur Mo $K\alpha$	
	255 K	245 K	175 K	100 K	35 K	10 K
Crystal data						
M_r	268.3	268.3	268.3	268.3	268.3	268.3
Crystal system, (super)space group	Orthorhombic, $Cmc2_1$	Orthorhombic, $Cmc2_1$	Monoclinic, $X2_1(\frac{1}{2}\frac{1}{2}\gamma)$	Monoclinic, $X2_1(\frac{1}{2}\frac{1}{2}\gamma)$	Monoclinic, $X2_1(\frac{1}{2}\frac{1}{2}\gamma)$	Monoclinic, $X2_1(\frac{1}{2}\frac{1}{2}\gamma)$
a, b, c (Å)	4.220243 (13), 15.10020 (5), 6.00012 (2)	4.218739 (13), 15.09850 (5), 6.00070 (2)	4.20914 (13), 15.08450 (5), 6.00165 (2)	4.201896 (13), 15.06749 (6), 6.00091 (2)	4.198482 (13), 15.05720 (10), 6.00025 (2)	4.198368 (14), 15.05560 (10), 6.00025 (2)
β (°)	90	90	90.051 (2)	90.0724 (2)	90.0843 (2)	90.0853 (2)
γ (Å^{-1})	–	–	0.39170	0.39350	0.39488	0.39487
V (Å^3)	382.36	382.2208	381.054 (9)	379.929 (3)	379.337 (3)	379.269 (3)
μ (mm^{-1})	14.47	15.49	15.52	15.59	13.56	13.41
Crystal size	0.06 × 0.03 × 0.002	0.06 × 0.03 × 0.002	0.06 × 0.03 × 0.002	0.06 × 0.03 × 0.002	0.06 × 0.03 × 0.002	0.18 × 0.14 × 0.12
$hklm_{min} - hklm_{max}$	$\bar{5}\,\bar{2}\,0\,\bar{8} - 5\,2\,0\,8$	$\bar{5}\,\bar{2}\,0\,\bar{8} - 5\,2\,0\,8$	$\bar{6}\,\bar{2}\,\bar{1}\,\bar{9}\,\bar{2} - 6\,2\,1\,9\,2$	$\bar{6}\,\bar{2}\,\bar{1}\,\bar{9}\,\bar{2} - 6\,2\,1\,9\,2$	$\bar{7}\,\bar{2}\,\bar{5}\,\bar{9}\,\bar{2} - 3\,25\,10\,2$	$\bar{6}\,\bar{2}\,\bar{5}\,\bar{10}\,\bar{2} - 3\,25\,10\,2$
Data collection						
Data collection method	STOE IPDS 2	STOE IPDS 2	STOE IPDS 2	STOE IPDS 2	Oxford Diffraction CCD	Oxford Diffraction CCD
Absorption correction	Numerical	Numerical	Numerical	Numerical	Gaussian	Gaussian
T_{min}, T_{max}	0.544, 0.753	0.474, 0.779	0.539, 0.752	0.531, 0.750	0.232, 0.446	0.218, 0.338
No. of measured, independent and observed [$I > 3\sigma(I)$] reflections	1643, 599, 593	1396, 607, 587	15 788, 7181, 4553	19 367, 7518, 6031	13 885, 5816, 5316	19 876, 6397, 5633
Extinction coefficient	190 (30)	1070 (180)	150 (50)	210 (40)	110 (30)	20 (17)
$R_{int}>3\sigma$	0.0684	0.1055	0.0776	0.0718	0.0340	0.0404
R_{int}(all)	0.0685	0.1056	0.0918	0.0740	0.0343	0.0407
Refinement						
R(obs), wR(obs)	0.0396, 0.0544	0.0467, 0.0543	0.0581, 0.0477	0.0450, 0.0407	0.0473, 0.0650	0.0416, 0.0488
R(all), wR(all)	0.0399, 0.0545	0.0477, 0.0543	0.1011, 0.0524	0.0606, 0.0426	0.0508, 0.0653	0.0485, 0.0496
g.o.f(all)	4.54	3.92	1.61	1.63	2.51	1.76
g.o.f(obs)	4.56	3.99	1.85	1.74	2.61	1.84
No. of reflections	599	607	7181	7518	5816	6397
No. of parameters	37	37	95	104	81	89
No. of reflections obs/all	593, 599	587, 607	7181, 4553	7518, 6031	5816, 5316	6397, 56 534
$\Delta\rho_{max}$, $\Delta\rho_{min}$ (e Å^{-3})	1.14, −1.77	7.41, −5.53	7.78, −7.80	6.58, −5.45	8.86, −7.34	5.19, −5.71
Absolute structure	Inversion twin tested	Inversion twin tested	Inversion twin tested	Inversion twin tested	Inversion twin tested	Inversion twin tested
Flack parameter	0.00 (3)	0.00 (6)	0.00 (4)	0.00 (7)	0.02 (6)	0.02 (6)
Main reflections (m = 0)						
No. of reflections obs/all	–	–	950, 989	1007, 1038	847, 864	920, 944
R(obs), wR(obs)	–	–	0.0324, 0.0378	0.0255, 0.0317	0.0241, 0.0307	0.0214, 0.0260
R(all), wR(all)	–	–	0.0339, 0.0378	0.0266, 0.0318	0.0245, 0.0307	0.0220, 0.0261
Satellite refections (m = 1)						
No. of reflections obs/all	–	–	3065, 4136	3717, 4332	3021, 3274	3249, 3593
R(obs), wR(obs)	–	–	0.0746, 0.0706	0.0497, 0.0459	0.0478, 0.0527	0.0430, 0.0430
R(all), wR(all)	–	–	0.1077, 0.0781	0.0633, 0.0483	0.0519, 0.0531	0.0498, 0.0438
Satellite reflections (m = 2)						
No. of reflections obs/all	–	–	538, 2056	1307, 2148	1445, 1678	1484, 1860
R(obs), wR(obs)	–	–	0.1442, 0.1662	0.0940, 0.0943	0.1061, 0.1594	0.0924, 0.1192
R(all), wR(all)	–	–	0.2979, 0.2178	0.1437, 0.1051	0.1120, 0.1596	0.1097, 0.1208

temperature until at 50 K, approximately coinciding with the onset of the intermediate magnetic phase (Yoshimura *et al.*, 2006), its largest value is reached (approximately 0.395 Å^{-1}). Below this temperature the γ component hardly varies any

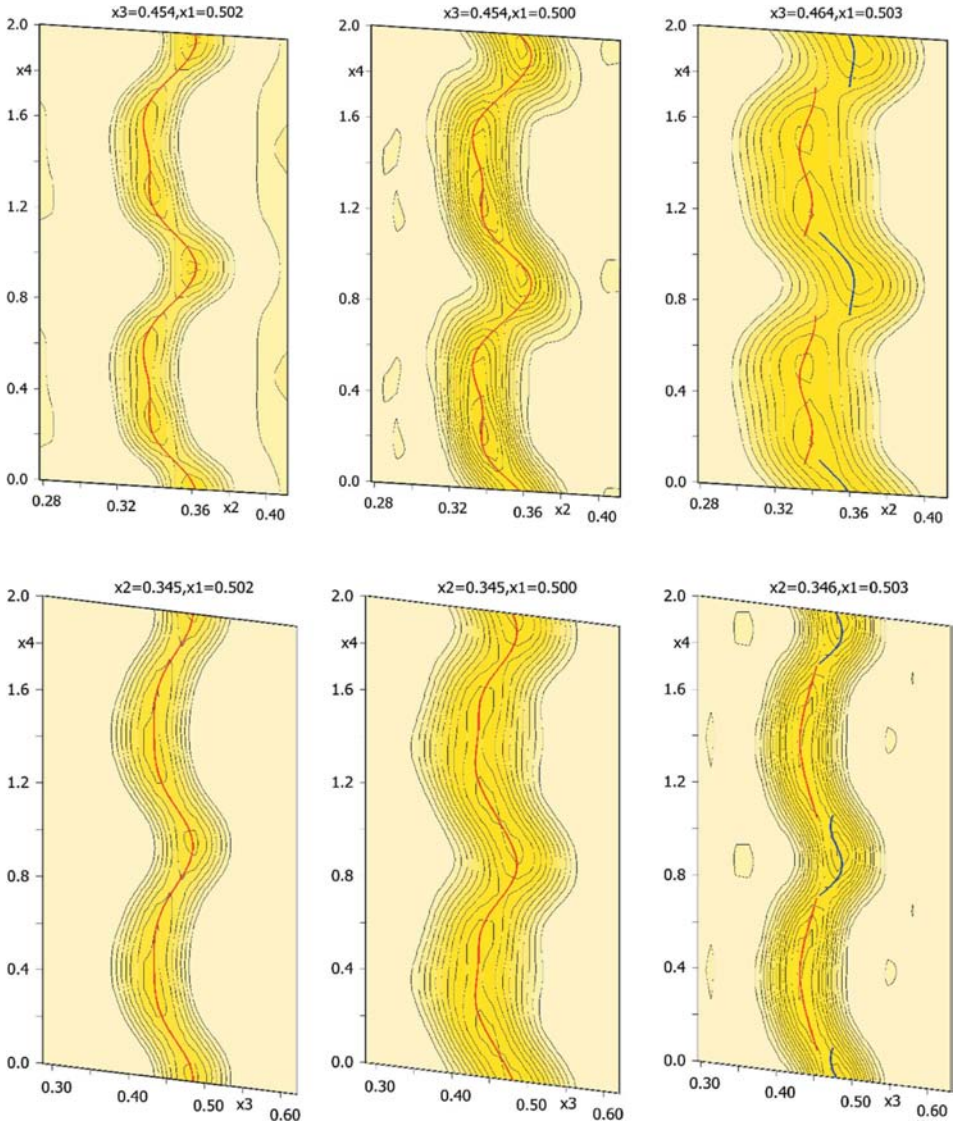

Figure 7
F(obs)–Fourier close to the Ba-atom positions at 100, 35 and 10 K ($\Delta x = \Delta y = \Delta z = 2$ Å); the centre of the *F*(obs) map at 10 K is at the averaged position of the two Ba atoms related by the crenel function.

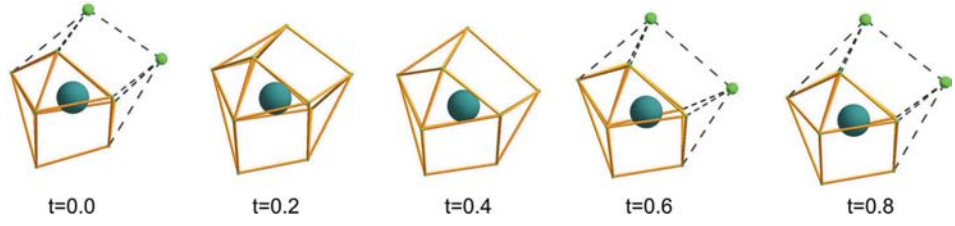

Figure 8
The coordination of Ba in $BaMnF_4$ at 10 K. Coordination polyhedra are shown for some selected values of *t*.

further and assumes a plateau-like behaviour, still maintaining its irrational value down to 10 K (Fig. 6).

If we analyze the development of the modulated structure of $BaMnF_4$ both as a function of the internal parameter *t* and as a function of temperature, the following major characteristics can be singled out:

(i) The character of the modulation function on Ba assumes a more anharmonic nature with decreasing temperature. This is clearly reflected in Fig. 7, which represents the electron density map around Ba at temperatures of 100, 35 and 10 K. While down to 35 K harmonics of third order are sufficient to describe the modulation, at 10 K the introduction of a crenel function using two atoms is superior. The width of the crenels is clearly different for the two atoms (approximately 2/3 for Ba1 and 1/3 for Ba2). However, the introduction of the crenel is only necessary in two directions (*x*2 and *x*3); identical coordinates *x*1 can be kept for the two Ba ion positions.

(ii) The coordination of Ba by oxygen varies strongly as a function of the internal parameter *t* and the shape of the coordination polyhedra change considerably (Fig. 8).

(iii) The average Mn—F distances in the octahedra vary smoothly as a function of temperature and *t*, and no abrupt changes are observed. This is also reflected in a very small fluctuation of the bond-valence sums of Mn. However, as can be seen in Fig. 9, for example, the octahedra do not behave as rigid units in the modulated structure at all as the variation of the individual Mn—F distances is considerable. A partial view of the modulated chain of MnF_6 octahedra at 10 K is shown in Fig. 10.

(iv) The behavior of the Mn—Mn distances, especially in the lowest-temperature region, deserves special attention, as the magnetic anomalies might be reflected in these distances. However, although the variation of distances is slightly increased with decreasing temperature (see Fig. 11), we do not observe any abrupt changes, which could be interpreted as a structural response to the magnetic ordering.

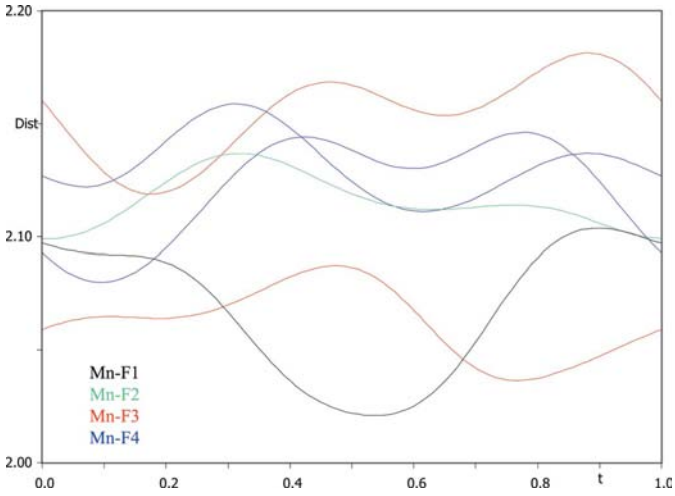

Figure 9
Mn—F distances in $BaMnF_4$ at 10 K as a function of *t*.

The question why $BaMnF_4$ forms a modulated structure while the other two compounds do not, might be answered on the basis of simple geometrical considerations.[4]

As already discussed earlier, the Mn ion has the largest ionic radius of all the ions known to be incorporated into the octahedra of this structure type (Fig. 2). As a consequence of the large size of the MnF_6 octahedra, the cavity in which the Ba ion is incorporated is also increased when compared with the Mg and Zn compounds. Indeed, a comparison of the volume of the polyhedra around Ba shows that it is approximately 5–6% larger in $BaMnF_4$ than in the other two compounds. This is also reflected in the fact that the bond-valence sums for Ba in $BaMnF_4$ are considerably lower at room temperature than in the other two compounds (Fig. 12, top).

We believe that in the two compounds with smaller octahedral cations ($BaZnF_4$ and $BaMgF_4$) the resulting cavity is well adapted to the atomic radius of Ba and thus the structures are stable down to 10 K. In $BaMnF_4$, on the other hand, the cavities get too large for the Ba ion at lower temperatures if the normal phase is maintained. This leads to the formation of the modulated structure in which the Ba coordination sphere is adjusted in such a way that the average bond-valence sums do not deviate too strongly from the ideal values. With further lowering of the temperature, the charge balance around the Ba ion can only be kept by introducing a strong anharmonic character of the modulation function for Ba, until finally at the lowest temperature this implies the formation of a crenel like modulation (Fig. 12, bottom).

5. Conclusions

Our investigations on the temperature-dependent behaviour of $BaMgF_4$, $BaZnF_4$ and $BaMnF_4$ demonstrate that the first two compounds are stable down to 10 K, while the third one undergoes a phase transition to an incommensurately modulated structure at approximately 250 K. The modulated phase is stable down to 10 K.

The magnetic anomalies observed in $BaMnF_4$ are exclusively reflected in the behavior of the γ component of the **q** vector, which assumes an irrational value of approximately 0.395 $Å^{-1}$ at the temperature corresponding to the onset of the magnetic ordering and then stays constant down to 10 K. Mn—Mn distances do not indicate any structural response to the magnetic ordering.

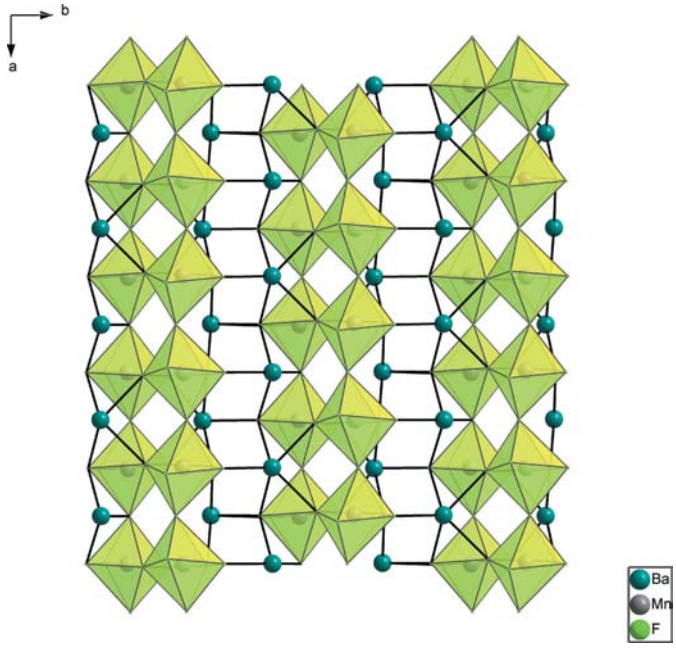

Figure 10
Partial view of the chains of octahedra in the modulated structure of $BaMnF_4$ at 10 K.

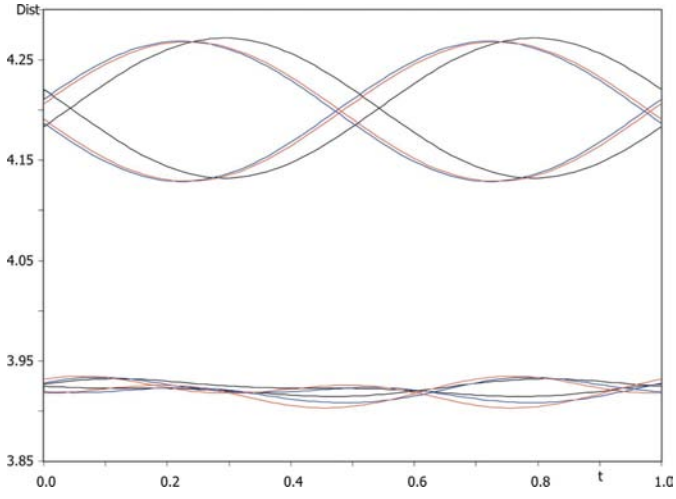

Figure 11
Mn—Mn distances at 100 (black), 35 (blue) and 10 K (red) as a function of *t*

[4] See also Yoshimura & Hidaka (2005) for a similar interpretation of the underlying reasons for the formation of the modulated structure

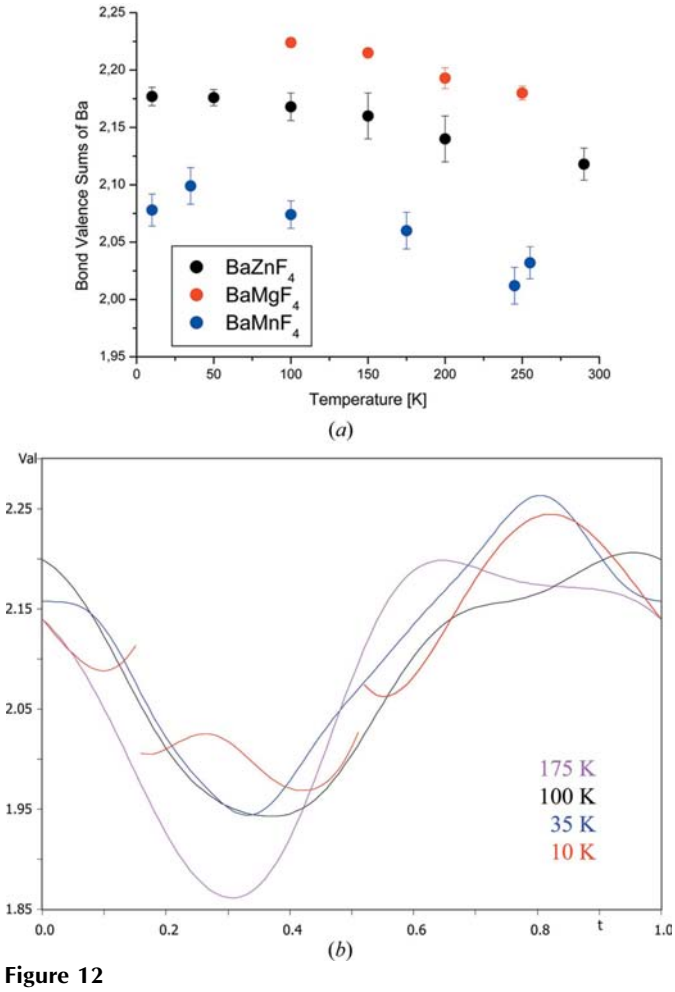

Figure 12
(*a*) Bond-valence sums of Ba in $BaMgF_4$, $BaZnF_4$ and $BaMnF_4$ as a function of temperature. For the modulated phase of $BaMnF_4$ average bond-valence sums are represented. (*b*) Bond-valence sums of Ba in $BaMnF_4$ as a function of *t*.

The transition to the modulated phase in $BaMnF_4$ can be explained assuming that the large size of the octahedral Mn ion implies an increase of the cavity in which the Ba ion is incorporated. This triggers the formation of the modulated structure at lower temperatures to adapt the coordination sphere around the Ba ion in such a way that the bond-valence sums remain close to the ideal value.

The crystals investigated were grown by J.-Y. Gesland (University of LeMans). We thank E. H. Bocanegra (University of the Basque Country) for the calorimetry measurements. We thank A. N. Fitch and G. Buth for their support of the synchrotron experiments performed at the ESRF, Grenoble, and Anka, Karlsruhe, respectively. H. Krüger, University of Innsbruck, was helpful during the measurement of the low-temperature data on $BaMgF_4$. Pablo Vitoria from the SGIker of the University of the Basque Country was of great help in carrying out the He-temperature measurements. We acknowledge financial support by the Spanish Ministerio de Educación y Ciencia, the Ministerio de Ciencia y Innovación (FIS2008-03834) and the Gobierno Vasco. JMP thanks the University of the Basque Country for a predoctoral scholarship. This work was supported by the European Community Research Infrastructure Action under the FP6-Programs: *Structuring the European Research Area*, through the Integrated Infrastructure Initiative *Integrating Activity on Synchrotron and Free Electron Laser Science* (IA-SFS).

References

Almairac, R., Bordallo, H. N., Bulou, A. & Nouet, J. (1995). *Phys. Rev. B*, **52**, 9370–9376.
Almairac, R., Bordallo, H. N., Bulou, A., Nouet, J. & Currat, R. (1997). *Phys. Rev. B*, **55**, 8249–8256.
Bordallo, H. N., Bulou, A., Almairac, R. & Nouet, J. (1994). *J. Phys. Condens. Matter*, **6**, 10365–10376.
Didomenico, M., Eibschutz, M., Guggenheim, H. J. & Camlibel, I. (1969). *Solid State Commun.* **7**, 1119–1125.
Ederer, C. & Spaldin, N. (2006). *Phys. Rev. B*, **74**, 024102.
Gingl, F. (1997). *Z. Anorg. Allg. Chem.* **623**, 705–709.
Gredin, P., Pierrard, A., Samouel, M., de Kozak, A. & Sean, C. R. H. (1996). *Acad. Sci. Ser. II*, **323**, 865–871.
Hidaka, M., Yoshimura, M., Nishimori, H., Fujii, H., Choi, J., Park, Y., Park, J. & Lee, K. (2001). *Phase Transitions*, **73**, 503–522.
Holmes, L., Eibschutz, M. & Guggenheim, H. J. (1969). *Solid State Commun.* **7**, 973–976.
Kannan, C. V., Shimamura, K., Zeng, H. R., Kimura, H., Villora, E. G. & Kitamura, K. (2008). *J. Appl. Phys.* **104**, 114113.
Keve, E. T., Abrahams, S. C. & Bernstein, J. L. (1969). *J. Chem. Phys.* **51**, 4928–4936.
Lapasset, J., Bordallo, H., Almairac, R. & Nouet, J. (1996). *Z. Kristallogr. New Cryst. Struct.* **211**, 934–935.
Müller, B. & Hoppe, R. (1972). *Mater. Res. Bull.* **7**, 1297–1306.
Petříček, V., Dušek, M. & Palatinus, L. (2006). *JANA*2006. Academy of Sciences of the Czech Republic, Praha.
Ryan, T. W. (1986). *J. Phys. C*, **19**, 1097–1106.
Samara, G. A. & Scott, J. F. (1977). *Solid State Commun.* **21**, 167–170.
Schaefer, F. J., Kleemann, W. & Tsuboi, T. (1983). *J. Phys. C*, **16**, 3987–4002.
Schnering, H. von & Bleckmann, P. (1968). *Naturwissenschaften*, **55**, 342–343.
Sciau, Ph., Lapasset, J., Grebille, D. & Berar, J. F. (1988). *Acta Cryst.* B**44**, 108–116.
Scott, J. F. (1979). *Rep. Prog. Phys.* **12**, 1075–1082.
Stephens, P. W. (1999). *J. Appl. Cryst.* **32**, 281–289.
Tsuboi, T. & Kleemann, W. (1983). *Phys. Rev. B*, **27**, 3762–3779.
Veira, J. R., Argyriou, D. N., Kiefer, K., Wolter, A. U. B., Alber, D., Meissner, M., Almairac, R., Reechuis, M. & Bordallo, H. N. (2008). *Phys. Rev. B*, **78**, 054104.
Villora, E. G., Shimamura, K., Jing, F., Medvedev, A., Tekekawa, S. & Kitamura, K. (2007). *Appl. Phys. Lett.* **90**, 192909.
Welsch, M., Kummer-Doerner, S., Peschel, B. & Babel, D. (1999). *Z. Anorg. Allg. Chem.* **625**, 1255–1260.
Werner, F. & Kubel, F. (2005). *J. Chem. Crystallogr.* **35**, 457–462.
Yoshimura, M. & Hidaka, M. (2005). *J. Phys. Soc. Jpn*, **74**, 1181–1189.
Yoshimura, M., Hidaka, M., Mizushima, T., Sakurai, J., Tsuboi, T. & Kleemann, W. (2006). *J. Magn. Magn. Mater.* **299**, 404–411.
Zeng, H., Shimamura, K., Villora, E. G., Takekawa, S. & Kitamura, K. (2007). *J. Appl. Phys.* **101**, 074109.